

ON THE CHEMODYNAMICS OF WOLF-RAYET RING NEBULAE: NGC 6888

CÉSAR ESTEBAN AND JOSÉ M. VÍLCHEZ

Instituto de Astrofísica de Canarias, 38200 La Laguna, Tenerife, Spain

Received 1991 July 17; accepted 1991 October 7

ABSTRACT

We have made a chemodynamical study of the W-R ring nebula NGC 6888 around the WN6 star WR 136. The observations combine, for the first time, high spatial and spectral resolution covering most of the optical range in different zones of the nebula.

The spectra show an emission system with three different velocity components: (1) $V_{\text{LSR}} = -64 \text{ km s}^{-1}$, (2) $V_{\text{LSR}} = +78 \text{ km s}^{-1}$, and (3) $V_{\text{LSR}} = +18 \text{ km s}^{-1}$. Components (1) and (2) correspond to the blue and red-shifted parts of the shell, and (3) is probably associated to the ambient ionized gas. The spectrum of each component has been extracted in order to study its ionization structure and excitation mechanism. Diagnostic diagrams indicate that the observed spectra are typical of purely photoionized nebulae, without any significant contribution of shock excitation. Chemical abundances of O/H, N/H, and He/H have been derived for each velocity component, finding that while the ambient gas has nearly solar abundances, the expanding shell presents a remarkable O/H deficiency, and strong overabundances of N/H and He/H. We conclude that this nebula is composed mostly of stellar ejecta, possibly produced by an event of very high mass loss or shell ejection at, or very near to, the RSG stage of the progenitor of WR 136 with an initial mass in the range 25–40 M_{\odot} .

Subject headings: ISM: abundances — ISM: individual (NGC 6888) — ISM: kinematics and dynamics — stars: Wolf-Rayet

1. INTRODUCTION

The recent spectroscopical observations of W-R ring nebulae with spatial or spectral resolution show that, in most cases, these objects are not homogeneous (Smith et al. 1988; Dufour, Parker & Henize 1988; Goudis, Meaburn, & Whitehead 1988; Vílchez & Esteban 1991), presenting different components possibly related to different epochs in the evolution of the mass-losing star and/or inhomogeneities in the ejection mechanisms or in the ambient interstellar medium (ISM). This paper attempts to shed some light on the evolution of W-R nebulae, investigating whether there is any coupling between chemical enrichment and velocity field in a prototype object of this class, NGC 6888, combining for the first time chemical and kinematical information in order to perform a chemodynamical study.

We have chosen the W-R ring nebula NGC 6888 to apply the chemodynamical method mainly because of its relatively high surface brightness and well-defined structure, in addition, its velocity field implies one of the highest expansion velocities reported for this kind of object. Marston & Meaburn (1988) determined an expansion velocity of 85 km s^{-1} for the shell of NGC 6888 and suggested that the central emission component of its spectrum is not related to the nebula itself. This emission should come from ISM along the line of sight to NGC 688 that is being ionized by hot OB stars, probably from the nearby Cygnus OB1 association.

NGC 6888 surrounds the WN 6 star WR 136, and it was formerly cataloged by Chu, Treffers, & Kwitter (1983) as a wind-blown bubble generated by swept-up ISM. Kwitter (1981) performed spatially resolved spectroscopy of the nebula, finding nitrogen and helium abundances higher than the ISM ones. She also claimed that, on the basis of this enrichment, the nitrogen- and helium-rich wind from the central star has contributed with $\approx 10\%$ of the observed nebular mass, and there-

fore the derived abundances should reflect the mixing up of interstellar and stellar wind material.

However, from the theoretical point of view, it is still not well understood how both materials can mix to produce the observed abundance anomalies (Weaver et al. 1977; Dyson & Smith 1985), and therefore an ejecta origin for the enriched gas seems a more likely explanation. The CCD imagery carried out by Dufour (1989) indeed points in this direction; these observations show an outer [O III] ring enveloping the whole [N II]-bright shell that forms the main body of the nebula. This morphology can only be explained by an ejecta inside a large wind-blown bubble, as seems to be the case in RCW 58 (Smith et al. 1988).

The observations are described in the following section. The results and their discussion are presented in § 3, and our main conclusions are summarized in § 4.

2. OBSERVATIONS

The observations were carried out in 1989 August at the Observatorio del Roque de los Muchachos (La Palma) with the 2.5 m Isaac Newton Telescope (INT) and the Intermediate Dispersion Spectrograph (IDS) at the Cassegrain focus, using the 235 mm camera with the IPCS (Image Photon Counting System) as detector. The configuration used was of 2040 pixels by 112 rows, with a pixel size of $15 \mu\text{m}$ in the dispersion direction and $50 \mu\text{m}$ in the spatial direction.

We obtained two-dimensional frames for three different slit positions along the major axis of the nebula, covering three different spectral ranges for each position: (1) from $\lambda 3600$ to $\lambda 4200$ with a resolution in velocity of 36 km s^{-1} FWHM and a typical exposure time of 5400 s taken with the H 2400B grating; (2) from $\lambda 4000$ to $\lambda 5050$ with 62 km s^{-1} FWHM resolution, and 3600 s exposure, using the 1200B grating; and (3) from $\lambda 5700$ to $\lambda 6800$, with a resolution of 45 km s^{-1} FWHM and

exposure time of 4500 s, using the 1200Y grating. The spatial coverage of the slit was always the same, 2.8, with a resolution of 1.5 pixel⁻¹. The seeing was about 1" throughout the observations.

From the three slit positions available, we have extracted one-dimensional spectra selecting those zones where each velocity component was seen more clearly. This was done in order to isolate each component more easily, minimizing the errors in the Gaussian fitting and any possible contamination by other components. All the selected zones are shown in Figure 1 (Plate 10). Zones A and B were extracted from the slit position shown in Figure 2 (Plate 11)—zone A from pixels 1 to 60 (90") and B from pixels 82 to 90 (14")—and correspond to the blue- and redshifted components of the shell respectively. Position C, with an extension of 16", shows a spectrum dominated by the central velocity component; it was extracted from a zone almost free of contribution from the bubble components.

Data reduction was performed at the IAC using a VAX 8350 with the standard software package FIGARO (Shorridge 1990). All the frames were wavelength-calibrated, sky subtracted, and extinction-corrected in two dimensions. Flux calibration in two dimensions was achieved by comparison with the standard stars Ross 640 (Oke 1976) and BD +48°2211 (Stone 1977). The DIPSO package (Howarth & Murray 1990) allowed the velocity analysis to be made via Gaussian fitting of the complex emission lines.

3. RESULTS AND DISCUSSION

Radial velocities and line intensities were obtained via Gaussian fitting of the lines from the selected flux-calibrated one-dimensional spectra. The reddening coefficient $C(H\beta)$ was derived using the quotients $H\gamma/H\beta$ and $H\delta/H\beta$ from the spectra taken in the yellow range ($\lambda\lambda 400\text{--}5050$). We could have used the $H\alpha$ flux but preferred not to do that because it comes from a different frame and also to prevent a possible systematic error in the absolute flux calibration from affecting the determination of $C(H\beta)$. Line intensity ratios for the blue and red spectral ranges were determined with respect to the brightest Balmer line present in each range ($H\delta$ for the blue and $H\alpha$ for the red). Line ratios were finally given with respect to $H\beta$ multiplying by the expected case B quotients $H\delta/H\beta$ and $H\alpha/H\beta$ and corrected for reddening using the derived $C(H\beta)$. Discrepancies between $H\delta$ fluxes measured in the yellow and blue parts are within 15%; in the case of $H\alpha$, the discrepancy between the measured flux and the value extrapolated from the Balmer yellow lines is typically within 30%.

The spectra were calibrated in wavelength up to an accuracy of ± 3 km s⁻¹. For the three zones selected, the three velocity components measured give the following V_{LSR} : -64 km s⁻¹, $+18$ km s⁻¹ and $+78$ km s⁻¹. The first and last correspond to the blueshifted and receding parts of the shell, while the 18 km s⁻¹ component can be related to the ambient ionized gas as suggested by Marston & Meaburn (1988) and Chu (1988). Our derived values for the velocity are in very good agreement with those reported by Marston & Meaburn (1988) and Lozinskaya et al. (1988) for the central parts of the bubble. An important difference between the shell and the ambient component is evident in Figure 2: while the shell components present a very clumpy appearance, the ambient component has a uniform brightness along the slit, and it is always present in all our slit positions.

Figure 3 shows a portion of a representative spectrum cen-

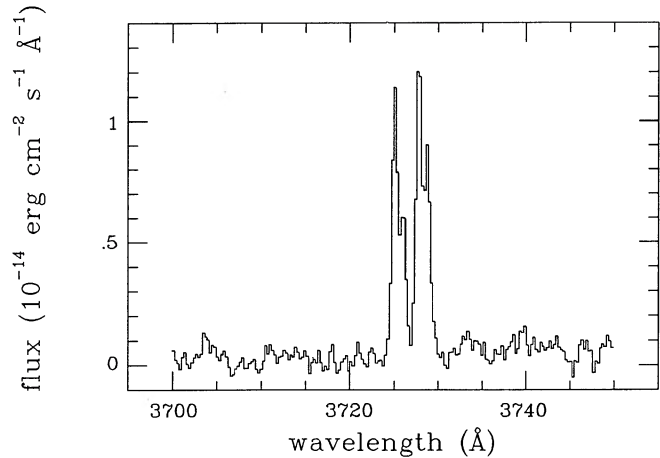


FIG. 3.—Representative part of a spectrum showing the [O II] $\lambda\lambda 3726, 3729$ doublet for the blueshifted part of the bubble and for the ambient gas. It was extracted from the pixels 16–30 of the slit position shown in Fig. 2.

tered in the density indicator [O II] $\lambda\lambda 3726, 3729$ with each line split into two velocity components. Emission profiles of the most important lines are presented in Figure 4 for several zones along the slit position illustrated in Figure 2, in order to map the spatial behavior of the ionization structure with respect to the velocity field of the nebula.

In Table 1 we show dereddened line intensity ratios with respect to $H\beta = 100.0$ for each velocity component, along with their corresponding $C(H\beta)$ and integrated $H\beta$ flux. Line fluxes were measured using the DIPSO package (Howarth & Murray 1990) via Gaussian fitting of the emission lines for each velocity component. Errors in the line flux measurements come from the uncertainties in the Gaussian fitting given by DIPSO. Colons, in Table 1, indicate relative errors $\geq 40\%$. The estimated uncertainty in $C(H\beta)$ for the blueshifted component is about 0.15 dex; for the other two velocity components, the nominal values given for the reddening must be taken only as an indication, due to the faintness of their spectra. The low value of the reddening coefficient obtained for the blue component—similar also to the nominal value found for the ambient gas—suggests that, in fact, this part of the shell is free of any substantial associated extinction. The somewhat larger extinction of the redshifted component could indicate a small absorption certainly produced by dust in the line of sight to the receding shell. This is also suggested by the fact that the redshifted emission is found always to be fainter than the corresponding blueshifted one, a possible consequence of the distribution of the absorbing material. We have compared our reddening determinations with previous work in the literature by Kwitter (1981). The value of $C(H\beta) = 0.72$ for zone 1E-KP in her paper, the nearest one to our regions A and B, compares well with the values derived in this work (see Table 1) taking into account the different observational set-ups and errors.

We have investigated the excitation mechanism making use of diagnostic diagrams (Sabbadin, Minello, & Bianchini 1977; Dopita & Evans 1986). For the spectra analyzed, no evidence of significant shock excitation has been found, indicating the photoionized nature of the nebula, at least in the zones observed. On these diagrams, the spectra of the shell produce [N II]/ $H\alpha$ line ratios that are outside the H II region box and entering the extended planetary nebulae locus. This behavior can be understood taking into account the nitrogen enrich-

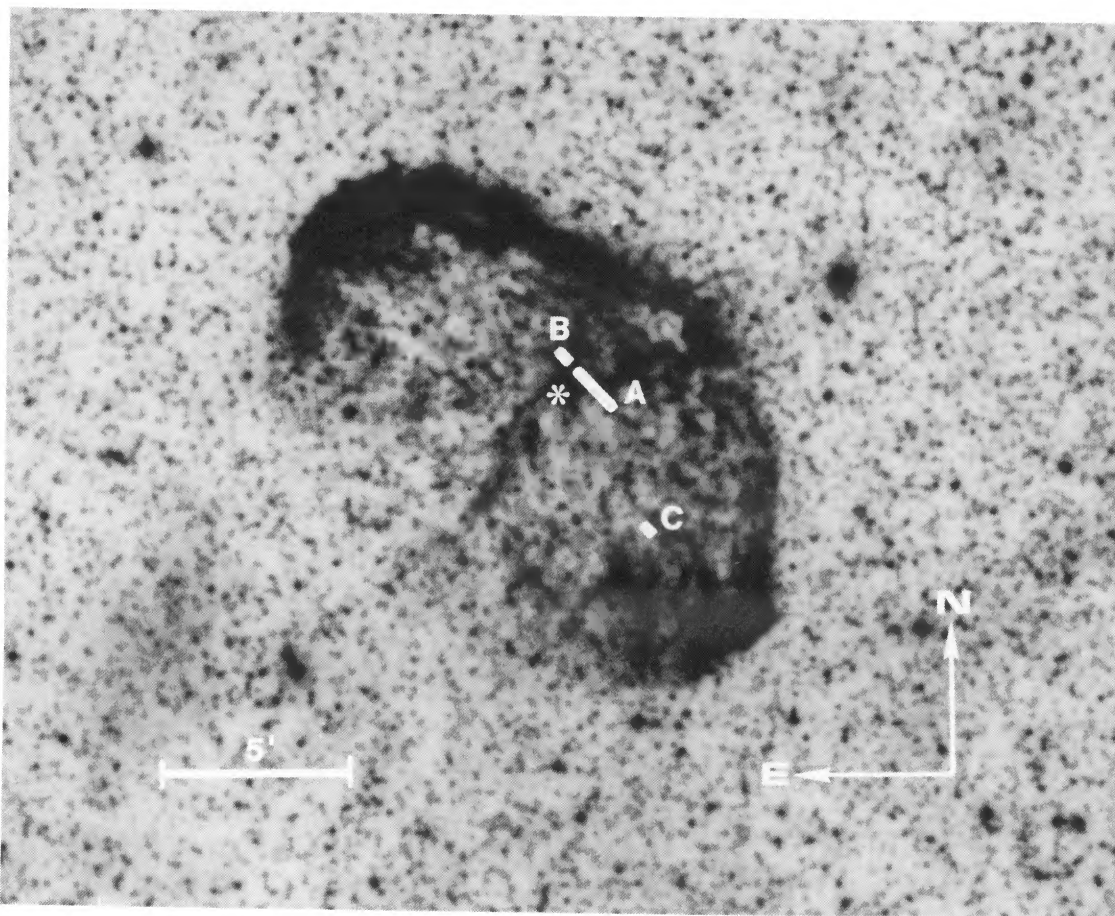


FIG. 1.—Image of NGC 6888 from the POSS blue plate. The labeled areas represent the different regions studied in our analysis.

ESTEBAN & VÍLCHEZ (see 390, 537)

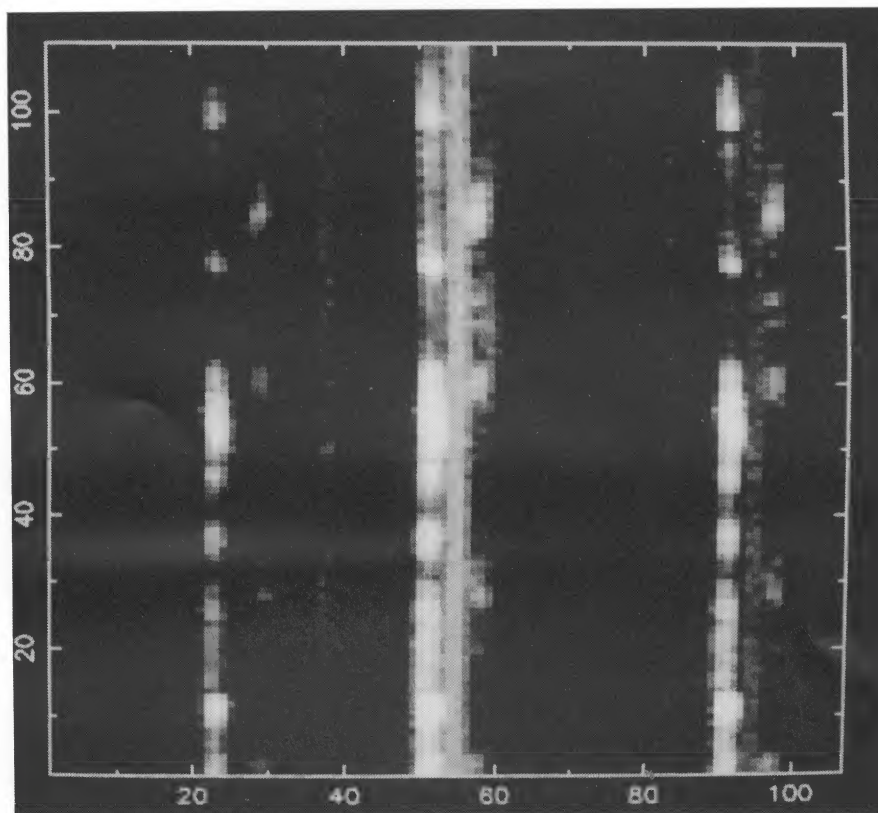


FIG. 2.—A logarithmic representation of a two-dimensional spectrum in the red range showing $H\alpha$ and $[N\ II]\ \lambda\lambda 6548$ and 6584 and the total spatial extension of a slit position taken for the central parts of the nebula.

ESTEBAN & VÍLCHEZ (see 390, 537)

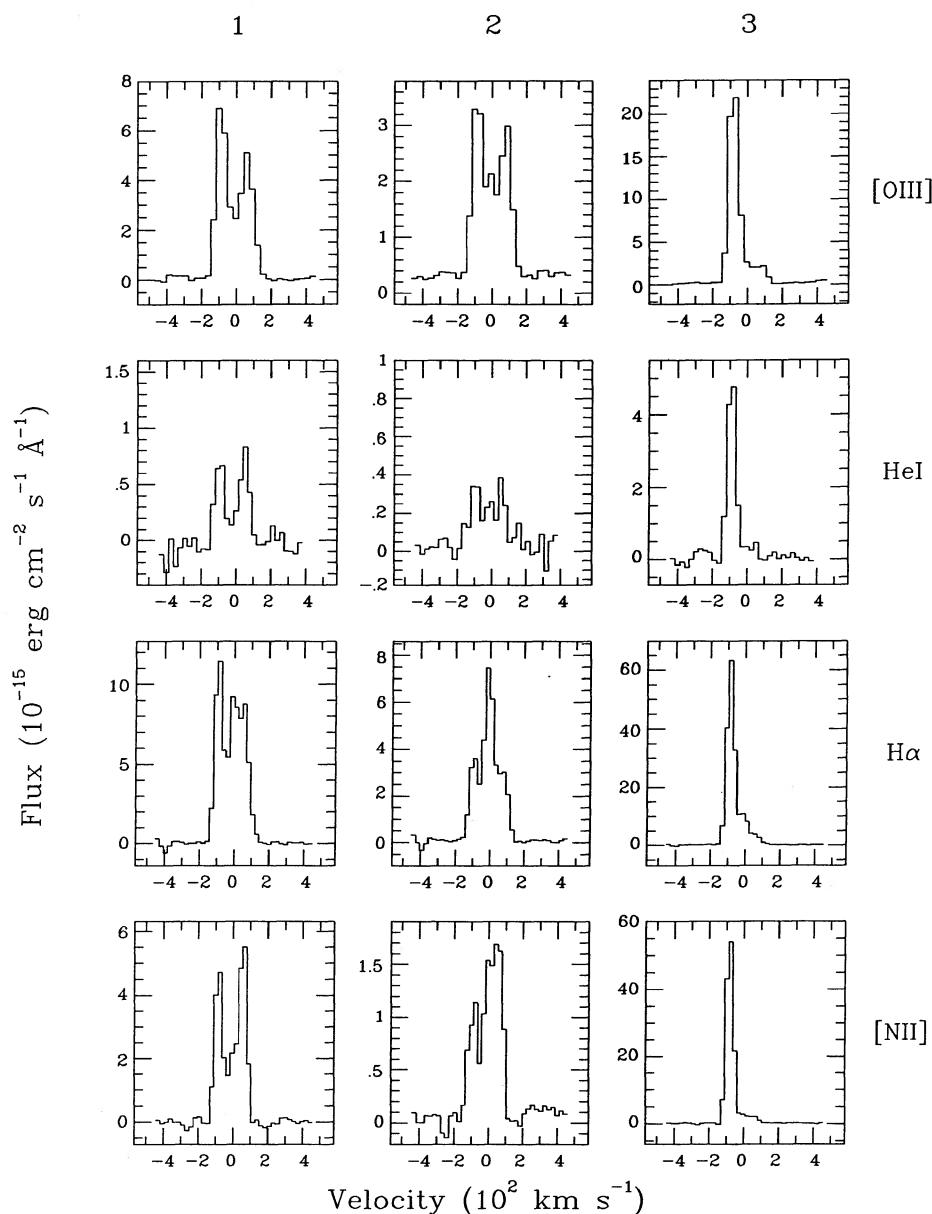


FIG. 4.—Emission-line profiles of [O III] $\lambda 5007$, He I $\lambda 5876$, H α , and [N II] $\lambda 6584$ at three different locations on slit position shown in Fig. 2 (row 1 corresponds to pixels 46–60, row 2 to pixels 65–75, and row 3 to pixels 76–90). The abscissa gives radial velocity ($V_R = V_{LSR} + 19.5 \text{ km s}^{-1}$).

ment of the nebula. On the other hand, the ambient spectrum appears entirely consistent with those of typical H II regions.

Electron temperatures have been derived via the usual [O III] and [N II] line ratios (Aller 1984) for the blueshifted component. For the other components it was impossible to obtain a direct measurement of the temperature due to their faintness. For the receding part of the shell, we assumed the value obtained for the blueshifted component; the strong similarity of both spectra suggest that this assumption may be correct. For the ambient gas spectrum we have estimated a mean electron temperature using the empirical method (Pagel et al. 1979). The electron density was derived using the [O II] and [S II] line ratios when it was possible; the derived values are coincident for the bubble components, being about 350 cm^{-3} in both cases. In contrast, the values for the ambient gas

are always at the low-density limit. The quoted values of the electron temperature and density, for the bubble components, are consistent with the previous values reported by Kwitter (1981), specially for her zone 1E-KP, the nearest to our regions A and B.

Abundances for the most important ions have been calculated using the formulae given by Aller (1984). He⁺/H⁺ ratios were computed as weighted means for those components with more than one useful He I line; for all these lines, we have computed collisional corrections following Clegg (1987), finding that they are negligible in all cases. Total abundances were determined following the normally adopted ionization correction scheme (see Diaz et al. 1987). Values for the electron temperature and density, as well as the ionic and total abundances for each velocity component, are presented in Table 2.

TABLE 1
LINE INTENSITY RATIOS

LINE (λ)	$f(\lambda)$	V_{LSR}		
		-64 km s ⁻¹	+18 km s ⁻¹	+78 km s ⁻¹
3705 He I	0.26	2.2:
3726 [O II]	0.26	18.8 ± 2.8	34 ± 10	12.3:
3729 [O II]	0.26	21.8 ± 3.3	52 ± 13	23.4:
3756 He I	0.26	2.4:
3798 H10	0.26	2.1:
3820 He I	0.25	2.2:
3835 H9	0.24	6.1 ± 1.3
3869 [Ne III]	0.23	9.3 ± 1.1	...	8.1:
3889 He I, H8	0.22	22.9 ± 1.8	18:	27.3 ± 8.2
3965 He I	0.21	0.8:
3967 [Ne III]	0.21	2.8 ± 1.0
3970 He I	0.21	11.2 ± 1.2	11	...
4009 He I	0.20	0.9:
4026 He I	0.20	3.4 ± 0.9
4101 H δ	0.18	24.7 ± 1.2	24 ± 5	26.2 ± 7.9
4340 H γ	0.135	47.2 ± 1.4	46 ± 7	48.5 ± 8.2
4363 [O III]	0.13	1.2:
4471 He I	0.10	8.2 ± 1.2	...	9.3:
4658 [Fe III]	0.05	2.8 ± 1.0
4861 H β	0.00	100.0 ± 1.0	100 ± 10	100.0 ± 18.0
4922 He I	-0.01	2.3 ± 1.0
4959 [O III]	-0.02	74.2 ± 1.5	32 ± 9	88.3 ± 22.1
5007 [O III]	-0.03	222.8 ± 1.1	105 ± 7	277.8 ± 27.8
5016 He I	-0.03	2.5 ± 0.8
5755 [N II]	-0.21	2.2 ± 0.7
5876 He I	-0.23	25.1 ± 1.8	14 ± 3	29.3 ± 4.4
6300 [O I]	-0.30	...	78 ± 10	...
6312 [S III]	-0.30	1.2:	...	5.2 ± 1.6
6363 [O I]	-0.31	...	24 ± 5	...
6548 [N II]	-0.34	72.2 ± 2.2	15 ± 5	60.5 ± 6.0
6563 H α	-0.34	287.0 ± 1.4	286 ± 20	286.7 ± 11.5
6584 [N II]	-0.34	228.6 ± 2.3	60 ± 15	177.7 ± 10.7
6678 He I	-0.35	7.4 ± 1.1	...	8.0 ± 2.4
6717 [S II]	-0.36	7.5 ± 1.3	35 ± 7	9.1 ± 2.7
6731 [S II]	-0.36	6.8 ± 1.2	20 ± 5	8.1 ± 2.4
$F(\text{H}\beta) \times 10^{-14}$...	4.44	0.23	0.19
$c(\text{H}\beta)$...	0.28	0.27	0.50

Errors in the ionic abundances have been estimated by taking into account the uncertainties in the electron temperature and errors in the line ratios used.

Two different abundance patterns are clear from the table, one corresponding to the shell and the other to the ambient ionized gas. The ambient gas has nearly solar abundances of O/H, N/H and He/H, and therefore it can be taken as an in situ reference for the local ISM abundances. The shell, on the other hand, present a deficiency of O/H by a factor of 4 with respect to the ISM; in contrast, N/H appears enhanced by a factor of 6, as well as helium, which is found to be overabundant by a factor of 2. The S/H abundance can be calculated for the redshifted component and appears roughly solar. This enrichment pattern clearly points out the stellar nature of the nebular material, and to estimate its relative importance, we made a simple calculation of an upper limit to the ratio of the mass of swept-up interstellar gas to the mass ejected by the star. Following the procedure outlined in Esteban et al. (1991), comparing the mass fractions of oxygen in the ejecta and in the ISM with those observed in the shell we find that this ratio is $M_{\text{ISM}}/M_{\text{ej}} \leq 0.3$. This result indicates that a significant fraction of NGC 6888 can be considered as material ejected from the central star WR 136, in at least 77% of its total ionized mass.

TABLE 2
PHYSICAL PARAMETERS AND ABUNDANCES

PARAMETER	V_{LSR}		
	-64 km s ⁻¹	+18 km s ⁻¹	+78 km s ⁻¹
$t([\text{O III}])$	0.95:	...	0.95: ^a
$t([\text{N II}])$	0.84 ± 0.10	...	0.84 ± 0.10 ^a
$\langle t \rangle^b$...	0.65	...
12 + log O ⁺⁺ /H ⁺	7.98 ± 0.25	8.39	8.07 ± 0.32
12 + log O ⁺ /H ⁺	7.54 ± 0.34	8.53	7.48:
12 + log O/H	8.11 ± 0.28	8.75	8.17:
log N ⁺ /O ⁺	0.29 ± 0.30	-1.10	0.25:
12 + log N/H	8.40 ± 0.35	7.65	8.42:
12 + log S ⁺ /H ⁺	5.71 ± 0.23	6.68	5.79 ± 0.29
12 + log S ⁺⁺ /H ⁺	7.17 ± 0.40
12 + log S/H	7.18 ± 0.40
log Ne ⁺ /O ⁺⁺	-0.92 ± 0.30	...	-1.07 ± 0.35
12 + log He ⁺ /H ⁺ (4471)	11.21 ± 0.07	...	11.27:
12 + log He ⁺ /H ⁺ (5876)	11.25 ± 0.04	11.00	11.32 ± 0.07
12 + log He ⁺ /H ⁺ (6678)	11.24 ± 0.07	...	11.27 ± 0.12
12 + log <He/H>	11.24 ± 0.06	11.00	11.30 ± 0.09
log Ne ([O II])	2.48	<2	...
log Ne ([S II])	2.57	<2	2.53

^a Assumed value; see text.

^b Value from the empirical calibration.

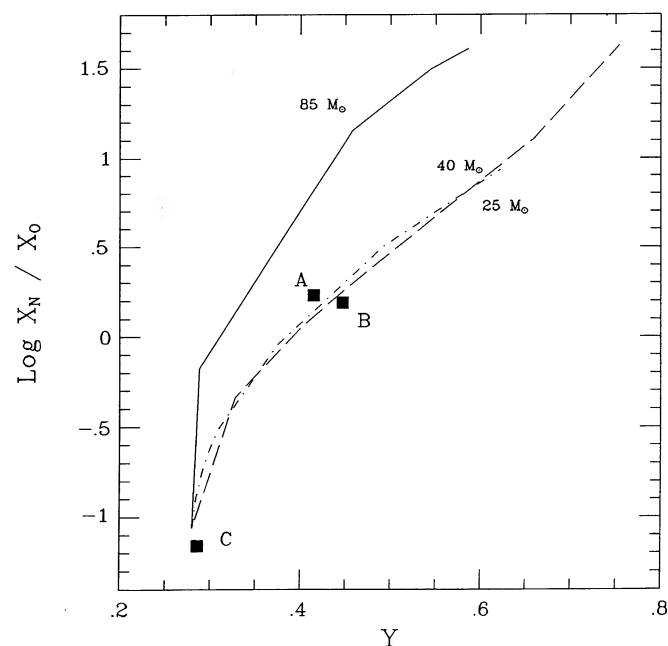


FIG. 5.—The ratio of nitrogen to oxygen mass fractions vs. the helium mass fraction. Lines represent the model predictions by Maeder (1990) for solar metallicity. The squares are our observational points for each velocity component. The processed nature of the shell gas is evident, in contrast to the ambient gas, and its good correlation with the expectations for a star with initial mass between 25 and 40 M_{\odot} at an intermediate point along its evolution to the W-R phase, is also clear.

We have made a crude comparison between the enrichment pattern observed and the predicted nucleosynthesis in the evolutionary models for massive stars by Maeder (1990). These models predict the evolution of surface abundances from the zero age main sequence to the end of the central carbon-burning phase. Our results for this nebula (see Fig. 5) indicate a range of overabundances of nitrogen and helium that, for models with initial masses between 25 and 40 M_{\odot} and solar metallicity, would correspond to evolutionary phases previous to the onset of the W-R stage. Considering the stellar nature of the nebular material, their observed overabundances are quite similar to the values expected in the models at, or very near to, the end of the RSG phase in the mass range considered. We then propose that shell ejection or an event of very high mass loss close the RSG phase, could be a plausible explanation for the origin of the enriched material.

4. SUMMARY

Results from a spectroscopical study of the W-R ring nebula NGC 6888 are presented. The observations combine, for the first time, high spatial and spectral resolution covering most of the optical range in different zones along the nebula, allowing us to analyze the physical conditions and chemical abundances for each velocity component.

The spectra of the central parts of the nebula show emission at three different velocities: (1) $V_{\text{LSR}} = -64 \text{ km}^{-1}$, (2) $V_{\text{LSR}} = +78 \text{ km}^{-1}$, and (3) $V_{\text{LSR}} = +18 \text{ km}^{-1}$. Components (1) and (2) are clearly identified as the blue- and redshifted parts of the expanding shell, while (3) must be related to the ambient interstellar component.

Comparison of the observed line ratios with diagnostic diagrams indicates that photoionization is, by far, the most important excitation mechanism for the zones observed, without any significant evidence of shock excitation.

The reddening coefficient, electron temperature, and density have been derived or estimated for each component. We find a somewhat higher reddening for the redshifted emission than for the other components, suggesting the presence of absorbing material inside or in the walls of the shell. Density, temperature and abundances in the shell and in the ambient gas appear to be quite different. While the ambient gas has nearly solar abundances, the shell appears to be deficient in O/H by a factor of 4 with respect to the local ISM, and strongly overabundant in N/H and He/H by factors of 6 and 2 respectively, while S/H remains unaltered. A stellar nature, for a large fraction of the shell gas, is concluded by this remarkable abundance pattern.

A comparison with model predictions of surface abundances by Maeder (1990), for solar metallicity, indicates that the abundances of the ejected material would correspond to an evolutionary stage previous to the onset of the W-R phase, for an initial stellar mass in the range 25–40 M_{\odot} . We propose that shell ejection close the RSG phase could be a plausible explanation for the origin of the enriched material.

We want to thank G. Tenorio-Tagle for very useful comments and suggestions on a first version of the paper. The INT is operated on the island of La Palma by the RGO at the Spanish Observatorio del Roque de los Muchachos of the Instituto de Astrofísica de Canarias.

REFERENCES

- Aller, L. H. 1984, *Physics of Thermal Gaseous Nebulae* (Dordrecht: Reidel)
 Clegg, R. E. S. 1987, *MNRAS*, 229, 31P
 Chu, Y.-H. 1988, *AJ*, 100, 986
 Chu, Y.-H., Treffers, R. R., & Kwitter, K. B. 1983, *ApJS*, 53, 937
 Díaz, A. I., Terlevich, E., Pagel, B. E. J., Vílchez, J. M., & Edmunds, M. G. 1987, *MNRAS*, 226, 19
 Dopita, M. A., & Evans, I. N. 1986, *ApJ*, 307, 431
 Dufour, R. J. 1989, *Rev. Mexicana Astron. Af.*, 18, 87
 Dufour, R. J., Parker, R. A. R., & Henize, K. G. 1988, *ApJ*, 327, 859
 Dyson, J. E., & Smith, L. J. 1985, in *Cosmic Gas Dynamics*, ed. F. D. Khan (Utrecht: VNU Science Press), 173
 Esteban, C., Vílchez, J. M., Smith, L. J., & Manchado, A. 1991, *A&A*, 244, 205
 Goudis, C. D., Meaburn, J., & Whitehead, M. J. 1988, *A&A*, 191, 341
 Howarth, I. D., & Murray, J. 1990, *SERC Starlink User Note*, No. 50
 Kwitter, K. B. 1981, *ApJ*, 245, 154
 Lozinskaya, T. A., Lomovskii, A. I., Pravdikova, V. V., & Surdin, V. G. 1988, *Soviet Astron. Lett.*, 14, 385
 Maeder, A. 1990, *A&AS*, 84, 139
 Marston, A. P., & Meaburn, J. 1988, *MNRAS*, 235, 391
 Oke, J. B. 1974, *ApJS*, 27, 21
 Pagel, B. E. J., Edmunds, M. G., Blackwell, D. E., Chun, M. S., & Smith, G. 1979, *MNRAS*, 189, 95
 Sabaddin, F., Minello, S., & Bianchini, A. 1977, *A&A*, 60, 147
 Shorridge, K. 1990, *SERC Starlink User Note*, No. 86
 Smith, L. J., Pettini, M., Dyson, J. E., & Hartquist, T. W. 1988, *MNRAS*, 234, 625
 Stone, R. P. S. 1977, *ApJ*, 218, 767
 Vílchez, J. M., & Esteban, C. 1991, in *IAU Symp. 143, Wolf-Rayet Stars and Interrelations with Other Massive Stars in Galaxies*, ed. K. van der Hucht & B. Hidayat (Dordrecht: Kluwer), 379
 Weaver, R., McCray, R. A., Castor, J., Shapiro, P., & Moore, R. 1977, *ApJ*, 218, 377